

GENERATING A MORPHABLE MODEL OF EARS

Reza Zolfaghari, Nicolas Epain, Craig T. Jin, Joan Glaunès, Anthony Tew

ABSTRACT

This paper describes the generation of a morphable model for external ear shapes. The aim for the morphable model is to characterize an ear shape using only a few parameters in order to assist the study of morphoacoustics. The model is derived from a statistical analysis of a population of 58 ears from the SYMARE database. It is based upon the framework of large deformation diffeomorphic metric mapping (LDDMM) and the vector space that is constructed over the space of *initial momentums* describing the diffeomorphic transformations. To develop a morphable model using the LDDMM framework, the initial momentums are analyzed using a kernel based principal component analysis. In this paper, we examine the ability of our morphable model to construct test ear shapes not included in the principal component analysis.

Index Terms— Morphable model, Ears, Currents, Shape analysis

1. INTRODUCTION

This paper describes a morphable model for external ear shapes. Our objective in creating the morphable model is to assist research into the prediction of individualized 3D audio filters for listeners based on the shape of their ears. The significance of the morphable model is its ability to compress the representation of 3D ear shapes to a set of parameters typically obtained by projection onto a set of orthogonal base functions [1, 2]. This parameterisation of ear shapes using a morphable model greatly aids in the study of morphoacoustics [3, 4, 5, 6], where the goal is to understand the link between variations in the shape of an ear and their effect on the corresponding set of 3D audio filter functions, referred to as head related impulse responses (HRIRs). HRIRs vary for each listener because each listener has differently shaped ears. There is an HRIR filter for each ear and each direction in space and these HRIR filters enable the rendering of binaural 3D audio for a listener.

Modeling ear shapes is a challenging task and ear shape deformations are arguably best described using a Riemannian space. In this regard, large deformation diffeomorphic metric mapping (LDDMM) is a framework to perform non-rigid diffeomorphic registration and mapping between images, surfaces, curves and distributions in two and three dimensional space [7, 8, 9, 10, 11, 12]. Diffeomorphic maps provide a smooth, invertible, one-to-one transformation between the source and target shape. In particular, considerable work has been undertaken to formulate an algorithm for mapping 3D triangulated surfaces [13, 14]. In a recent paper [15] we show how LDDMM coupled with fast multipole boundary element method (FM-BEM)

simulations can assist with the study of morphoacoustics and in [16] we show how a template ear shape can be estimated using LDDMM. The template ear is a critical element of our morphable model, but we leave the description of its calculation to [16] as it is beyond the focus of this paper. While LDDMM permits a multiscale approach to mapping ear shapes as discussed in [16], the morphable model presented here is based on single scale LDDMM transformations. In this work we use the LDDMM framework combined with a kernel based principal component analysis (KPCA) technique [17, 18, 19] to construct a morphable model for ears. In particular, our morphable model uses the concept of the linear space of *initial momentums* [20] within the framework of LDDMM and a set of coupled differential equations known as the “shooting equations” to construct and model ears. We use the SYMARE database of ears described in [21] for generating our morphable model. This paper describes the morphable model and examines its ability to reconstruct new ear shapes, *i.e.*, ear shapes outside of the database used for constructing the model.

2. METHODS

2.1. LDDMM Framework

LDDMM [22, 12] is a mathematical framework that can be employed for the registration and morphing of three-dimensional shapes [14, 13]. It is based on theories from functional analysis, variational analysis and reproducible kernel Hilbert spaces. In the LDDMM framework we model a 3D-shape as a mesh with triangular faces, which we refer to as $S(\mathbf{X})$ where \mathbf{X} is the matrix specifying the mesh vertices and S represents the mesh connectivity (the triangular faces). We now describe two fundamental LDDMM operations that are at the core of this work. The first operation, referred to as LDDMM mapping, consists in determining the diffeomorphic transformation that morphs an initial shape $S_1(\mathbf{X})$, with $\mathbf{X} \in \mathbb{R}^{N \times 3}$, into a target shape $S_2(\mathbf{Y})$ with $\mathbf{Y} \in \mathbb{R}^{M \times 3}$. The result of this operation is a set of vectors, $\{\alpha_n(0)\}_{1 \leq n \leq N}$, defined at the vertices \mathbf{X} and known as the *initial momentum* vectors, that characterize the diffeomorphic transformation entirely. The second operation, referred to as geodesic shooting, applies the morphing operation (*i.e.* the diffeomorphic flow) described by the initial momentum vectors to a given shape.

2.1.1. LDDMM mapping

LDDMM models the mapping or morphing of $S_1(\mathbf{X})$ to $S_2(\mathbf{Y})$ as a dynamic flow of diffeomorphisms of the ambient space, \mathbb{R}^3 , in which the surfaces are embedded. This flow of diffeomorphisms, $\phi^{\mathbf{v}}(t, \cdot)$, is defined via the partial differential equation:

$$\frac{\partial \phi^{\mathbf{v}}(t, \mathbf{X})}{\partial t} = \mathbf{v}(t) \circ \phi^{\mathbf{v}}(t, \mathbf{X}), \quad (1)$$

where $\mathbf{v}(t)$ is a time-dependent vector field, $\mathbf{v}(t) : \mathbb{R}^3 \rightarrow \mathbb{R}^3$ for $t \in [0, 1]$, which models the infinitesimal efforts of the flow, and \circ denotes function composition. Note that the superscript \mathbf{v} on $\phi^{\mathbf{v}}(t, \mathbf{X})$ simply denotes that the flow of diffeomorphisms is defined

R. Zolfaghari, N. Epain and C.T. Jin are with CARLab, School of Electrical and Information Engineering, The University of Sydney, Sydney, Australia. email: craig.jin@sydney.edu.au.

A. Tew is with the Department of Electronics, The University of York, Heslington, York, UK. email: tony.tew@york.ac.uk.

J.A. Glaunès is with the MAP5, Université Paris Descartes, Sorbonne Paris Cité 75006 Paris, France. email: alexis.glaunes@mi.parisdescartes.fr.

for a particular time-dependent vector field $\mathbf{v}(t)$. This vector field belongs to a Hilbert space of regular vector fields equipped with a kernel, k_V , and a norm $\|\cdot\|_V$ that models the infinitesimal cost of the flow. In the LDDMM framework, we determine $\mathbf{v}(t)$ by minimizing the cost function, J_{S_1, S_2} :

$$J_{S_1, S_2}(\mathbf{v}(t)) = \gamma \int_0^1 \|\mathbf{v}(t)\|_V^2 dt + E(S_1(\phi^{\mathbf{v}}(1, \mathbf{X})), S_2(\mathbf{Y})), \quad (2)$$

where E is a norm-squared cost measuring the degree of matching between $S_1(\phi^{\mathbf{v}}(1, \mathbf{X}))$ and $S_2(\mathbf{Y})$. In this work we use the Hilbert space of currents [8, 14] to compute E because it is easier and more natural than using landmarks. The parameter γ is a parameter that sets the relative weight of the two terms in the cost function. In this work $\gamma = 5 \times 10^{-5}$.

It can be shown that the time-dependent vector field, $\mathbf{v}(t)$, can be expressed as a sum of momentum vectors, $\alpha_n(t)$, with one momentum vector defined for each of the N vertices in \mathbf{X} :

$$\mathbf{v}(t) = \frac{d\mathbf{x}(t)}{dt} = \sum_{n=1}^N k_V(\mathbf{x}_n(t), \mathbf{x}(t)) \alpha_n(t), \quad (3)$$

where in this work we use the Cauchy kernel defined by:

$$k_V(\mathbf{x}, \mathbf{y}) = \frac{1}{1 + \frac{\|\mathbf{x} - \mathbf{y}\|^2}{\sigma_V^2}}, \quad (4)$$

for \mathbf{x} and \mathbf{y} in \mathbb{R}^3 . The σ_V parameter is a scale parameter that determines through the kernel, k_V , the range of influence of the momentum vectors $\alpha_n(t)$. Setting σ_V to a larger value increases the coupling in the motion of vertices that are further apart. In this work, $\sigma_V = 10$ mm. Further, the initial momentum vectors, $\alpha_n(0)$, determine the diffeomorphic mapping of S_1 to S_2 entirely [17]. In other words, S_2 can be represented as a deformation of S_1 through the diffeomorphic flow defined by the initial momentum vectors $\{\alpha_n(0)\}_{1 \leq n \leq N}$. In the following, we refer to the calculation of the initial momentum vectors as the mapping operation, \mathcal{M} :

$$\{\alpha_n(0)\}_{1 \leq n \leq N} = \mathcal{M}(S_1, S_2). \quad (5)$$

2.1.2. Geodesic Shooting

Geodesic shooting consists in using a set of initial momentum vectors, $\{\alpha_n(0)\}_{1 \leq n \leq N}$, to morph a shape S_1 into another shape, S_3 . This is done by solving the *shooting equations*, which couple the momentum vectors to the vertex positions across time and are given by:

$$\begin{aligned} \frac{d\alpha_r(t)}{dt} &= - \sum_{n=1}^N \langle \alpha_r(t), \alpha_n(t) \rangle \nabla_{\mathbf{x}_r(t)} (k_V(\mathbf{x}_r(t), \mathbf{x}_n(t))) \\ \frac{d\mathbf{x}_r(t)}{dt} &= \sum_{n=1}^N k_V(\mathbf{x}_n(t), \mathbf{x}_r(t)) \alpha_n(t) \end{aligned} \quad (6)$$

where $\langle \cdot, \cdot \rangle$ denotes the inner product in \mathbb{R}^3 and $\nabla_{\mathbf{x}(t)}(\cdot)$ denotes the gradient operator, further $1 \leq r \leq N$. Note that the initial conditions for Equations (6) are given by the initial positions and momentum vectors. In the following, we refer to the process of morphing shape S_1 into shape S_3 as the shooting operation, \mathcal{S} :

$$S_3 = \mathcal{S}(S_1, \{\alpha_n(0)\}_{1 \leq n \leq N}). \quad (7)$$

2.2. Kernel Based Principal Component Analysis (KPCA)

In the previous section, we have shown how a given shape could be represented as the deformation of another shape through a flow of diffeomorphisms. In order to build a morphable model of ear shapes, we represent every ear in a given population as a deformation of a unique template shape, T , which represents the population's *average* ear. Details regarding the calculation of such a template are described in [16]. In this work, we assume the template shape, T , is given. The first step in our analysis is to calculate the initial momentum vectors for every ear, S_i , in the population of L ears, as follows:

$$\{\alpha_n^{(l)}(0)\}_{1 \leq n \leq N} = \mathcal{M}(T, S_l) \quad (8)$$

Together with the template shape, the set of initial momentum vectors form a rudimentary model of ear shape such that the template shape can be morphed into any of the shapes in the population. In order to simplify this model, we apply a kernel based Principal Component Analysis (KPCA) to the deformations represented by the initial momentum vectors. We use the kernel version of PCA because the space of deformations is Riemannian.

In order to calculate the principal components, we calculate the covariance matrix, \mathbf{C} , which expresses the mutual correlation of the different ear shapes in the space of deformations. To compute this matrix we first construct a data matrix $\mathbf{A} \in \mathbb{R}^{3N \times L}$ which contains the initial momentum vectors for the entire population of ears:

$$\mathbf{A} = [\mathbf{a}_1, \mathbf{a}_2, \dots, \mathbf{a}_L]_{3N \times L} \quad (9)$$

where \mathbf{a}_l denotes the column vector containing all the initial momentum vector coefficients for shape S_l . We then center the data by subtracting the population average momentum vectors. The centered data matrix, $\hat{\mathbf{A}}$, is given by:

$$\hat{\mathbf{A}} = [\hat{\mathbf{a}}_1, \hat{\mathbf{a}}_2, \dots, \hat{\mathbf{a}}_L]_{3N \times L} \quad (10)$$

where $\hat{\mathbf{a}}_l$ is the vector of the centered momentum vectors for the l -th shape:

$$\hat{\mathbf{a}}_l = \mathbf{a}_l - \bar{\mathbf{a}} \quad \text{with} \quad \bar{\mathbf{a}} = \frac{1}{L} \sum_{i=1}^L \mathbf{a}_i. \quad (11)$$

We also form the kernel matrix, \mathbf{K} , which contains the values of the kernel function for every pair of vertex positions that comprise the vertices, \mathbf{X} , of the template shape T :

$$\begin{aligned} \mathbf{K} &= \begin{bmatrix} \mathbf{K}_{11} & \mathbf{K}_{12} & \dots & \mathbf{K}_{1N} \\ \mathbf{K}_{21} & \mathbf{K}_{22} & & \vdots \\ \vdots & & \ddots & \vdots \\ \mathbf{K}_{N1} & \dots & \dots & \mathbf{K}_{NN} \end{bmatrix}, \\ \mathbf{K}_{mn} &= k_V(\mathbf{x}_m, \mathbf{x}_n) \mathbf{I}_{3 \times 3}, \end{aligned} \quad (12)$$

where $\mathbf{I}_{3 \times 3}$ denotes the 3×3 identity matrix.

The correlation between two shapes is calculated as the inner product of the initial momentum vectors in the Hilbert space of deformations, V . The correlation between shapes S_i and S_j is given by:

$$c_{ij} = \left\langle \{\alpha_n^{(i)}(0)\}, \{\alpha_n^{(j)}(0)\} \right\rangle_V = \hat{\mathbf{a}}_i^T \mathbf{K} \hat{\mathbf{a}}_j, \quad (13)$$

where $(\cdot)^T$ denotes the transpose of a vector or matrix. Thus, the covariance matrix for the entire population of ears, \mathbf{C} , is given by:

$$\mathbf{C} = \hat{\mathbf{A}}^T \mathbf{K} \hat{\mathbf{A}} \quad (14)$$

In order to calculate the principal components, as well as the coordinates of the ears in the basis of the principal components, we perform the singular value decomposition of the covariance matrix \mathbf{C} :

$$\mathbf{C} = \mathbf{V}\mathbf{D}\mathbf{V}^T. \quad (15)$$

The matrix of the principal components, \mathbf{U} , can be then calculated as:

$$\mathbf{U} = \hat{\mathbf{A}}\mathbf{V}\mathbf{D}^{-\frac{1}{2}}. \quad (16)$$

Note that the principal components are orthogonal in the Hilbert space of deformations, *i.e.*, $\mathbf{U}^T\mathbf{K}\mathbf{U} = \mathbf{I}$. It follows from Equation (16) that $\hat{\mathbf{A}} = \mathbf{U}\mathbf{D}^{\frac{1}{2}}\mathbf{V}^T$ and therefore $\mathbf{D}^{\frac{1}{2}}\mathbf{V}^T$ provides the coordinates of the different ear shapes in the basis of the principal components. Each ear can thus be reconstructed by: (1) computing $\mathbf{a}_l = \bar{\mathbf{a}} + \mathbf{U}\mathbf{D}^{\frac{1}{2}}\mathbf{v}_l$ (\mathbf{v}_l is the l -th column of \mathbf{V}^T); and (2) shooting from the template in the \mathbf{a}_l direction, *i.e.*, $S_l = \mathcal{S}(T, \{\mathbf{a}_l\}_{1 \leq l \leq N})$. In other words, we now have a morphable model of ears in which each ear shape in the population is described by L parameters, where L is the size of the population of ears. Note that the dimension of the model can be further reduced at the cost of reduced shape reconstruction accuracy by keeping only the first Q ($Q \leq L$) principal components.

2.3. Morphable Model of Ears

We now describe how a new ear shape S_p , that was not included in the computation of the principal components, can be described using the KPCA data. The computation of the model parameters for S_p can be divided into three steps. First, compute the initial momentum vectors, \mathbf{a}_p , corresponding to the morphing of the template T into shape S_p . Second, the population average momentum vectors are subtracted from \mathbf{a}_p to obtain the centered initial momentum vectors, $\hat{\mathbf{a}}_p$. Third, the centered momentum vectors are projected onto the principal components to obtain the model parameters, $\tilde{\mathbf{v}}_p$. The procedure is summarized below:

Algorithm 1 Computation of the Model Parameters for an Ear

Inputs: $\mathbf{U}, \bar{\mathbf{a}}, S_p$.

- 1: $\{\alpha_n^{(p)}(t)\}_{1 \leq n \leq N} = \mathcal{M}(T, S_p)$
- 2: $\hat{\mathbf{a}}_p = \mathbf{a}_p - \bar{\mathbf{a}}$
- 3: $\tilde{\mathbf{v}}_p = \mathbf{U}^T\mathbf{K}\hat{\mathbf{a}}_p$
- 4: **return** $\tilde{\mathbf{v}}_p$

The reconstruction of shape S_p from the model parameters is performed in two steps. First, the initial momentum vectors for shape S_p are estimated by combining the principal components according to the model parameters. Second, the shooting operation is used to morph the template into \tilde{S}_p , an approximation of shape S_p . The shape reconstruction operation is summarized below:

Algorithm 2 Reconstruction of an Ear from the Model Parameters

Inputs: $T, \mathbf{U}, \tilde{\mathbf{v}}_p$.

- 1: $\hat{\mathbf{a}}_p = \bar{\mathbf{a}} + \mathbf{U}\tilde{\mathbf{v}}_p$
- 2: $\tilde{S}_p = \mathcal{S}(T, \{\hat{\mathbf{a}}_p\}_{1 \leq n \leq N})$
- 3: **return** \tilde{S}_p

Note that shape \tilde{S}_p is an approximation of S_p because: (1) the LDDMM operation $\mathcal{M}(T, S_p)$ does not match shapes perfectly; and (2) the principal components may not enable perfect reconstruction of the initial momentum vectors for shape S_p .

3. EXPERIMENTS

3.1. Experimental setup

A morphable model of ear shapes was created based on 58 different ear shapes from the SYMARE database [21]. While the SYMARE database is the largest database of its kind, 58 ears is not a large number considering the human population and it is unclear how well the morphable model can describe an arbitrary ear not included within the database. In order to address this issue, we repeatedly left one of the ears, S_i , out of the dataset of 58 ears and formed a morphable model based on the remaining 57 ears. We then examined the ability of the morphable model to reconstruct the ear that was left out. In other words, for each shape S_i in the dataset, we applied the KPCA analysis described in Section 2.2 using 57 ear shapes (*i.e.*, leaving S_i out). Then, using the method described in Section 2.3 an approximate ear shape \tilde{S}_i was reconstructed. We then examined how accurately the approximation \tilde{S}_i matches the original shape S_i using a shape difference analysis based on currents (please refer to the Appendix). Further, we examined the shape reconstruction accuracy as a function of the number of principal components used to reconstruct the ear shape. Note that in order to exclude the mismatch caused by the LDDMM matching procedure, we actually compared the \tilde{S}_i shapes to the shapes Z_i obtained by matching the template T to S_i and shooting using the true initial momentum vectors.

3.2. Results

Results are summarized in Figure 2. As expected the accuracy of the model improves as the number of principal components increases. However, there is very little difference between the results obtained with 50 and 57 principal components, which indicates that the last 7 principal components have very little influence on the accuracy of the model. Interestingly, the quality of the reconstruction strongly depends on the ear considered. Some ears are reconstructed with great accuracy using relatively few principal components, while others are poorly reconstructed using the full basis of principal components. This is illustrated in Figure 1 where examples of reconstructed ears are compared to the corresponding reference shapes. Observe that shapes Z_1 and Z_2 were reconstructed with no apparent mismatch, while there is clear mismatch for shapes Z_3 , Z_4 and Z_5 . In summary, these results indicate that the morphable model is promising, but requires a larger population of ears to enable the model to morph into any possible ear shape.

4. CONCLUSION

In this paper we have presented a method for generating a morphable model of ears using the LDDMM framework. The core idea of this method is to apply KPCA to the initial momentum vectors corresponding to morphing a template ear into the different ears in the dataset. We tested the method over a dataset of 58 ear shapes and examined how well each ear in this dataset would be reconstructed using a model formed with the 57 remaining ears. The results indicate that a larger dataset would be required to generate a model that can morph into any ear shape.

5. APPENDIX: ANALYSING SHAPE DIFFERENCE USING CURRENTS

In this appendix we describe a method for measuring the local mismatch between two ear shapes. This method is based on the represen-

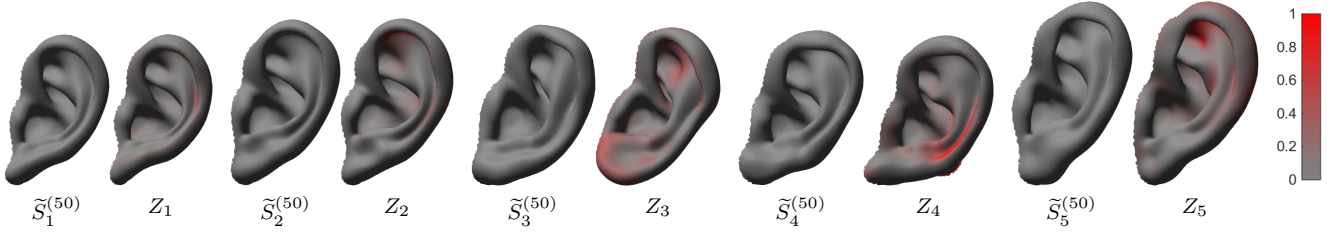


Fig. 1. This figure compares ear shapes reconstructed using 50 principal components, $\tilde{S}_i^{(50)}$, to the corresponding reference shapes Z_i . Colors (constant luminance, so examine online) on the shape indicate local shape mismatch calculated using the measure $\hat{d}(\tilde{S}_i^{(50)}, Z_i, f)$.

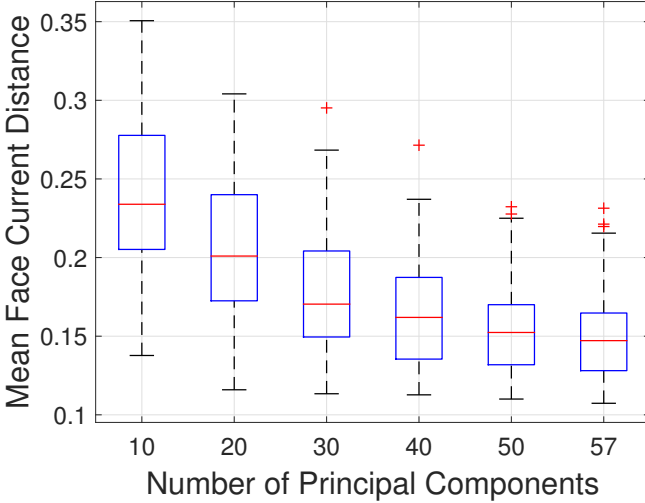


Fig. 2. The shape reconstruction accuracy of the model as a function of the number of principal components is shown. Red lines indicate the median value of $\bar{d}(\tilde{S}_i, Z_i)$, blue boxes indicate the interquartile range, whiskers indicate the whole data range and red crosses indicate outliers. Note that ear shape \tilde{S}_5 corresponds to the largest outlier for 30 and 40 principal components and that ear shape \tilde{S}_4 corresponds to the largest outlier for 50 and 57 principal components.

tation of surfaces as currents [14]. The current, $[S_1]$, corresponding to shape S_1 is characterized by a set of vectors, $\mathbf{n}_1(f)$, defined as follows: (1) there is one vector originating from the center, $\mathbf{c}_1(f)$, of each face f of S_1 ; (2) the vectors point outwards and are normal to the faces; (3) the norm of each vector is proportional to the area of the face. In order to examine the similarity between two shapes S_1 and S_2 for the region surrounding face f of S_1 we propose to use the measure $\hat{d}(S_1, S_2, f)$ given by:

$$\begin{aligned} \beta_1(f) &= \sum_g k_R(\mathbf{c}_1(f), \mathbf{c}_1(g)) \langle \mathbf{n}_1(f), \mathbf{n}_1(g) \rangle, \\ \beta_2(f) &= \sum_h k_R(\mathbf{c}_1(f), \mathbf{c}_2(h)) \langle \mathbf{n}_1(f), \mathbf{n}_2(h) \rangle, \\ d(S_1, S_2, f) &= |\beta_2(f) - \beta_1(f)|, \\ \hat{d}(S_1, S_2, f) &= \min\left(\frac{d(S_1, S_2, f)}{|\beta_1(f)|}, 1\right), \end{aligned} \quad (17)$$

where k_R denotes the Cauchy kernel and is defined as in Eq. (4) with a scale parameter $\sigma_R = 2$ mm. In Eq. (17), $\beta_1(f)$ corresponds to

the convolution of vector $\mathbf{n}_1(f)$ with every other vector $\mathbf{n}_1(g)$ in S_1 , while $\beta_2(f)$ corresponds to the convolution of $\mathbf{n}_1(f)$ with every vector $\mathbf{n}_2(h)$ in S_2 . When S_1 is very similar to S_2 in the vicinity of face f , $\beta_1(f)$ and $\beta_2(f)$ are almost equal and $d(S_1, S_2, f)$ is very small. On the other hand, when the two shapes are very dissimilar (orthogonal or far away from each other), $\beta_2(f)$ is very small and $d(S_1, S_2, f)$ is relatively large. In order to enable meaningful comparisons across different triangular faces and different shapes, we normalise $d(S_1, S_2, f)$ by the absolute value of $\beta_1(f)$. We also limit the maximum value of $\hat{d}(S_1, S_2, f)$ to unity to ensure the measure does not blow up when $\beta_1(f)$ is very small.

The overall similarity between two ear shapes is calculated as the average similarity measure, $\bar{d}(S_1, S_2)$, given by:

$$\bar{d}(S_1, S_2) = \frac{1}{F} \sum_{f=1}^F \hat{d}(S_1, S_2, f), \quad (18)$$

where F denotes the total number of faces in shape S_1 .

6. REFERENCES

- [1] V. Blanz and T. Vetter, "Face recognition based on fitting a 3d morphable model," *Pattern Analysis and Machine Intelligence, IEEE Transactions on*, vol. 25, no. 9, pp. 1063–1074, Sept 2003.
- [2] T. Cashman and A. Fitzgibbon, "What shape are dolphins? building 3d morphable models from 2d images," *Pattern Analysis and Machine Intelligence, IEEE Transactions on*, vol. 35, no. 1, pp. 232–244, Jan 2013.
- [3] A. Tew, C. Hetherington, and J. Thorpe, "Morphoacoustic perturbation analysis," in *Proceedings of the Joint meeting of the 11th Congrès Français d'Acoustique and the 2012 Annual Meeting of the Institute of Acoustics from UK*, Nantes, France, 2012, pp. 867–872.
- [4] D. Y. N. Zotkin, J. Hwang, R. Duraiswaini, and L. S. Davis, "Hrtf personalization using anthropometric measurements," in *Applications of Signal Processing to Audio and Acoustics, 2003 IEEE Workshop on*. Ieee, 2003, pp. 157–160.
- [5] C. Jin, P. Leong, J. Leung, A. Corderoy, and S. Carlile, "Enabling individualized virtual auditory space using morphological measurements," in *Proceedings of the First IEEE Pacific-Rim Conference on Multimedia (2000 International Symposium on Multimedia Information Processing)*. Citeseer, 2000, pp. 235–238.
- [6] P. Mokhtari, H. Takemoto, R. Nishimura, and H. Kato, "Pinna sensitivity patterns reveal reflecting and diffracting surfaces that

- generate the first spectral notch in the front median plane,” in *Acoustics, Speech and Signal Processing (ICASSP), 2011 IEEE International Conference on*. IEEE, 2011, pp. 2408–2411.
- [7] J. Glaunès, A. Trounev, and L. Younes, “Diffeomorphic matching of distributions: a new approach for unlabelled point-sets and sub-manifolds matching,” in *Computer Vision and Pattern Recognition, 2004. CVPR 2004. Proceedings of the 2004 IEEE Computer Society Conference on*, vol. 2, June 2004, pp. II–712–II–718 Vol.2.
- [8] J. Glaunès, A. Qiu, M. I. Miller, and L. Younes, “Large deformation diffeomorphic metric curve mapping,” *International Journal of Computer Vision*, vol. 80, pp. 317–336, 2008.
- [9] M. F. Beg, M. I. Miller, A. Trounev, and L. Younes, “Computing large deformation metric mappings via geodesic flows of diffeomorphisms,” *International Journal of Computer Vision*, vol. 61, no. 2, pp. 139–157, 2005.
- [10] P. Dupuis, U. Grenander, and M. Miller, “Variational problems on flows of diffeomorphisms for image matching,” *Quarterly of applied mathematics*, vol. 56, no. 3, p. 587, 1998.
- [11] M. Miller, A. Trounev, and L. Younes, “On the metrics and euler-lagrange equations of computational anatomy,” *Annual review of biomedical engineering*, vol. 4, no. 1, pp. 375–405, 2002.
- [12] M. Miller and L. Younes, “Group actions, homeomorphisms, and matching: A general framework,” *International Journal of Computer Vision*, vol. 41, no. 1, pp. 61–84, 2001.
- [13] M. Vaillant, A. Qiu, J. A. Glaunès, and M. I. Miller, “Diffeomorphic metric surface mapping in subregion of the superior temporal gyrus,” *NeuroImage*, vol. 34, no. 3, pp. 1149 – 1159, 2007.
- [14] M. Vaillant and J. A. Glaunès, “Surface matching via currents,” in *Information Processing in Medical Imaging*, ser. Lecture Notes in Computer Science, G. E. Christensen and M. Sonka, Eds. Springer Berlin Heidelberg, 2005, vol. 3565, pp. 381–392.
- [15] R. Zolfaghari, N. Epain, C. T. Jin, J. Glaunès, and A. Tew, “Large deformation diffeomorphic metric mapping and fast-multipole boundary element method provide new insights for binaural acoustics,” in *Acoustics, Speech and Signal Processing (ICASSP), 2014 IEEE International Conference on*, May 2014, pp. 2863–2867.
- [16] R. Zolfaghari, N. Epain, C. Jin, A. Tew, and J. Glaunès, “A multiscale lddmm template algorithm for studying ear shape variations,” in *Signal Processing and Communication Systems (ICSPCS), 2014 8th International Conference on*, Dec 2014, pp. 1–6.
- [17] M. Vaillant, M. Miller, L. Younes, A. Trounev *et al.*, “Statistics on diffeomorphisms via tangent space representations,” *NeuroImage*, vol. 23, no. 1, p. 161, 2004.
- [18] C. Cury, J. Glaunès, M. Chupin, and O. Colliot, “Analysis of anatomical variability using diffeomorphic iterative centroid in patients with alzheimer’s disease,” *Computer Methods in Biomechanics and Biomedical Engineering: Imaging & Visualization*, no. ahead-of-print, pp. 1–9, 2015.
- [19] C. Cury, “Statistical shape analysis of the anatomical variability of the human hippocampus in large populations.” Ph.D. dissertation, Université Pierre et Marie Curie-Paris VI, 2015.
- [20] M. Miller, A. Trounev, and L. Younes, “Geodesic shooting for computational anatomy,” *Journal of Mathematical Imaging and Vision*, vol. 24, no. 2, pp. 209–228, 2006. [Online]. Available: <http://dx.doi.org/10.1007/s10851-005-3624-0>
- [21] C. Jin, P. Guillon, N. Epain, R. Zolfaghari, A. van Schaik, A. Tew, C. Hetherington, and J. Thorpe, “Creating the sydney yolk morphological and acoustic recordings of ears database,” *Multimedia, IEEE Transactions on*, vol. 16, no. 1, pp. 37–46, Jan 2014.
- [22] U. Grenander and M. I. Miller, “Computational anatomy: An emerging discipline,” *Quarterly of applied mathematics*, vol. 56, no. 4, pp. 617–694, 1998.